Bioactive compounds immobilized on Ti and TiNbHf: AFM-based investigations of biofunctionalization efficiency and cell adhesion

C. Herranz-Diez,[a,b,†,††] Q. Li,[c,†] C. Lamprecht,[c] C. Mas-Moruno,[a,b,d] S. Neubauer,[e,f] H. Kessler,[e,f] J. M. Manero,[a,b,d] J. Guillem-Marti[a,b,d] and C. Selhuber-Unkel[*c]

[a] Biomaterials, Biomechanics and Tissue Engineering Group, Department of Materials Science and Metallurgical Engineering, Technical University of Catalonia (UPC), Spain.

[b] Biomedical Research Networking Centre in Bioengineering, Biomaterials and Nanomedicine (CIBER-BBN), Diagonal 647, 08028 Barcelona, Spain.

[c] Dept. Biocompatible Nanomaterials, Institute for Materials Science, University of Kiel, Kaiserstr. 2, D-24143 Kiel, Germany. E-mail: cse@tf.uni-kiel.de

[d] Centre for Research in NanoEngineering (CRnE)-UPC, c/Pacual i Vila 15, 08028 Barcelona, Spain.

[e] Institute for Advanced Study and Center for Integrated Protein Science, Department Chemie, Technische Universität München, Lichtenbergstr. 4, 85747 Garching, Germany.

[f] Max Planck Institute for Intelligent Systems, Heisenbergstr. 3, 70569 Stuttgart, Germany.

[*] corresponding author

† Authors contributed equally.

†† Present address: Academic Unit of Restorative Dentistry, School of Clinical Dentistry, University of Sheffield, Claremont Crescent, Sheffield S10 2TA, UK.

Total number of words: 5761

Total number of tables: 0

Total number of figures: 5

Keywords: Titanium alloy; recombinant protein; RGD peptide; cell adhesion; atomic forcemicroscopy; mesenchymal stem cell

Abstract

Implant materials require optimal biointegration, including strong and stable cell-material interactions from the early stages of implantation. Ti-based alloys with low elastic modulus are attracting a lot of interest for avoiding stress shielding, but their osseointegration potential is still very low. In this study, we report on how cell adhesion is influenced by linear RGD, cyclic RGD, and recombinant fibronectin fragment III_{8-10} coated on titanium versus a novel low-modulus TiNbHf alloy. The bioactive molecules were either physisorbed or covalently coupled to the substrates and their conformation on the surfaces was investigated with atomic force microscopy (AFM). The influence of the different bioactive coatings on the adhesion of rat mesenchymal stem cells was evaluated using cell culture assays and quantitatively analyzed at the single cell level by AFM-based single-cell force spectroscopy. Our results show that bioactive moieties, particularly fibronectin fragment III_{8-10}, improve cell adhesion on titanium and TiNbHf and that the covalent tethering of such molecules provides the most promising strategy to biofunctionalize these materials. Therefore, the use of recombinant protein fragments is of high importance for improving the osseointegration potential of implant materials.

Introduction

New materials for bone replacement have attracted increasing interest in recent years. In addition to designing materials with well-defined mechanical properties, biocompatibility and the ability to integrate into the surrounding living tissue are critical issues [1-4]. Titanium (Ti) and its alloys are currently some of the most important materials in bone replacement applications. They have excellent biocompatibility and osseointegration properties and are therefore very valuable materials for many different implant types [5-8].

In recent years, the TiNbHf ternary system has become very important among titanium alloys because of its excellent mechanical properties, which include a low modulus, high tensile strength and good biocompatibility [9]. Such a low modulus is very beneficial for improving shielding effect, which in the worst case can lead to implant failure. In this regard, we have recently developed a Ti25Nb21Hf alloy based on optimization of molecular orbital calculations of electronic structures towards a low modulus of elasticity and the potential for superelasticity [10-12]. The alloy is nickel and vanadium free, has improved biocompatibility and possesses a modulus of elasticity of 85 GPa [13, 14]. Although Ti and Ti-based alloys are well-established as materials for biomedical devices, tailored cell-material interactions, aimed at improving their bioactivity and long-lasting functionality, are still crucial and challenging tasks that require improvement. Particularly, TiNbHf alloys require biofunctionalization for facilitating cell adhesion at the early stages of implantation [15].

Surface functionalization can be used as a strategy to increase cell adhesion and osteoinduction on implant materials [16-18]. For example, implant surfaces can be functionalized with different types of bioactive coatings, such as extracellular matrix (ECM) proteins, recombinant fragments of ECM proteins, and short peptides that are recognized by cell adhesion molecules, such as integrins [19-22]. The immobilization of such molecules on a surface can either be achieved by physisorption or by covalent binding. For instance, silanization is a common technique to covalently immobilize small peptides and proteins on diverse surfaces. In particular, 3-aminopropyltriethoxysilane (APTES) has been shown to be a suitable silane for immobilizing molecules on Ti and its alloys [23, 24].

Although surface functionalization with bioactive motifs to improve the bioactivity and osteointegration of materials is well established [25, 26], each type of aforementioned biomolecules presents advantages and disadvantages. To mimic the natural conditions found in living tissue, material coatings based on native protein from the ECM should provide an optimal environment for cell attachment. Nevertheless, proteins are sensitive to pH and temperature changes, which disrupt the weak bonds between chains, causing proteins to lose their secondary structure and denature. Even the contact to surfaces can induce their denaturation, which in turn decreases or abolishes their bioactive function [27]. In order to avoid full-length protein structures that are prone to denaturation, an alternative is to mimic the adhesive function of ECM proteins by synthesizing their particular adhesion motifs. A prominent example is the short peptide sequence arginine-glycine-aspartic acid (RGD) [28, 29]. This short peptide sequence has been used to enhance cell adhesion on a variety of different surface types [15, 30, 31], even in *in vivo* studies [32, 33]. Although the binding affinity of RGD has strongly been improved by cyclization of the RGD sequence [34, 35], which is realized by adding flanking residues and constraining the conformation of the RGD motif to a loop [36, 37], the RGD binding sequence does not recapitulate the full functionality of ECM proteins. Native proteins contain multiple cell-binding sequences, which allow dynamic and simultaneous binding to cellular receptors and positively trigger cell adhesive events [38].

Hence, surfaces functionalized with RGD do not amplify cell adhesion as much as, for example, surfaces functionalized with fibronectin. Therefore, the use of recombinant proteins, which resemble fragments of fibronectin, has become more and more important in recent years [39], as it is much more convenient for a surface coating to use small protein fragments instead of large ECM proteins.

To evaluate the biointegration potential of implants and thus their effectiveness *in vivo*, it is essential to thoroughly investigate the mechanisms of cell adhesion on such surfaces after coating with different surface functionalization strategies. Previous studies have shown that cells distinguish between different adhesive substrates within only a few minutes of cell-substrate contact, indicating a strong impact of initial adhesion on the later progression of cell

adhesion [40]. Particularly, the quantification of cell adhesion with single-cell force spectroscopy has emerged as a valuable tool for characterizing cell-surface interactions in great detail [41, 42].

In this work, we carried out an atomic force microscopy (AFM) based evaluation of the conformation and cell adhesive function of bioactive molecules immobilized on Ti and TiNbHf. Linear RGD (linRGD), cyclic RGD (cRGD) and recombinant fragment of fibronectin ($FNIII_{8-10}$) were immobilized on the materials either by physisorption or silanization. The $FNIII_{8-10}$ fragment has been abbreviated as "CAS" because it encompasses the "cell attachment site" of the protein containing both RGD and PHSRN sequences. The success of functionalization was recorded by AFM topography measurements in combination with nanolithography. In order to quantify the biological potential of the different coating types chosen here, single-cell force spectroscopy was employed to investigate the adhesion strength of rat mesenchymal stem cells (rMSCs) for the very initial stage of cell-surface contact that is not accessible by optical or fluorescence-based methods. Furthermore, *in vitro* assays were carried out to investigate cell viability and to characterize actin stress fiber formation on the different surface types.

Material and Methods

Metal sample preparation

The Ti25Nb21Hf alloy was fabricated by vacuum arc melting at Fort Wayne Metals (Indiana, USA) as described in C. Herranz-Diez et al. [13]. Ti bar was purchased from Outokumpu (ASTM F 67, ISO 5832-2, Finland). Discs between 2 and 3 mm in thickness were cut from each bar and ground with wet grinding paper (320, 800, 1200 and 2500) followed by colloidal silica polishing (particle size 0.05 µm, from ATM GmbH) until achieving a mirror finish. Samples were cleaned in an ultrasound bath with cyclohexane (≥99.5%), isopropanol (≥99.7%), ethanol (≥99.5%), deionized water and acetone (≥99.9%) (all chemicals from Sigma-Aldrich, Germany).

Synthesis of bioactive compounds (CAS, linRGD, cRGD)

The fibronectin fragment CAS, which spans the 8-10th type III repeats of human fibronectin, was produced using standard recombinant DNA techniques. cDNA encoding CAS was ligated into a pGEX-6P-1 vector tagged with glutathione S-transferase (GST) and resistant to ampicillin (GE Healthcare, UK) forming a construct that was amplified in DH5α cells. After amplification, the construct was isolated from the cells and sequenced. BL21 cells were transformed with the correct construct, streaked onto an LB agar plate containing 100 µg/ml of ampicillin and incubated at 37 º C overnight. Colonies were isolated and dynamically cultured in LB broth with 100 µg/ml of ampicillin at 37 ºC. When the culture reached an absorbance value of $OD_{\lambda 600}$=0.6, 1 mM isopropyl β-D-1-thiogalactopyranoside (IPTG) was added to induce protein expression. After 4 h incubation, the cell broth was centrifuged at 7700 rpm for 10 min at 4 ºC, and the pellet was resuspended in 20 ml of PBS (Invitrogen). The suspension was sonicated with 8 time pulses (30 sec per pulse) with 1 min pause between each pulse. After sonication, 20% Triton X-100 was added and the suspension was incubated at 4 ºC for 30 min under mild agitation. The suspension was centrifuged at 12000 g for 10 min at 4 ºC. After centrifugation, the supernatant was purified by ÄKTApurifier (GE Healthcare equipment) using affinity columns GSTrap (GE Healthcare). Briefly, the column was equilibrated and washed with PBS. Then it was washed with PreScission Cleavage Buffer (50 mM Tris-HCl, 150mM NaCl, 1mM EDTA, 1mM dithiothreitol, pH 7.0). The GST was cleaved by HRV3C Protease (Sigma-Aldrich) overnight at 4 ºC with 10 cleavage units/mg of fusion protein. The purified product was verified as >95% pure FN III $_{8\text{-}10}$ by SDS-PAGE. Protein concentration was determined by a BCA assay (Pierce, Thermo Fisher Scientific, Rockford, IL, USA).

The linear peptide MPA-Ahx-Ahx-Ahx-Gly-Arg-Gly-Asp-Ser-OH (linRGD) (Ahx: aminohexanoic acid; MPA: 3-mercaptopropionic acid) was manually synthesized by solid-phase peptide synthesis (SPPS) following the Fmoc/tBu strategy[43] on 2-chlorotrityl chloride resin (Iris Biotech GmbH, Marktredwitz, Germany) as previously reported [44]. The purified peptide was characterized by analytical HPLC (Waters Alliance 2695 chromatography system; Waters, MA, USA) (10 to 40% MeCN over 8 min, t_R = 4.227 min) and mass spectrometry by

MALDI-TOF (Applied Biosystems, Foster City, CA, USA) (m/z calcd. for $C_{38}H_{67}N_{11}O_{13}S$: 917.46, found: 918.30 $[M+H]^+$; 940.28 $[M+Na]^+$); 956.25 $[M+K]^+$).

The cyclic peptide MPA-Ahx-Ahx-Ahx-cyclo(-RGDfK-) (cRGD) was synthesized as described elsewhere [34, 35, 45, 46]. In brief, the appropriately protected spacer-anchor unit MPA(Trt)-Ahx-Ahx-Ahx-OH and cyclo(-R(Pbf)GD(OtBu)fK-) were each synthesized by SPPS, and then coupled in solution using HATU and DIEA in presence of HOAt as coupling agents. Reaction work-up, side-chain deprotection and HPLC purification yielded the desired peptide: analytical HPLC (10 to 40 % MeCN over 8 min, t_R = 6.578 min) and MALDI-TOF (m/z calcd. for $C_{48}H_{78}N_{12}O_{11}S$: 1030.56, found: 1031.39 $[M+H]^+$; 1053.37 $[M+Na]^+$); 1069.35 $[M+K]^+$).

Sample silanization

For covalent binding of bioactive compounds, Ti and TiNbHf samples were coated with amino groups by silanization. The surface of the material was activated by a 5 min oxygen plasma treatment (TePla 100-E). Activated samples were immersed into a 0.08 M solution of aminopropyl-triethoxysilane (APTES, Sigma-Aldrich) in toluene (Sigma-Aldrich) at 70 ºC for 1 h under agitation. After silanization, samples were sonicated in toluene for 5 minutes and washed with toluene (3x), acetone (1x), isopropanol (3x), distilled water (3x), ethanol (3x) and acetone (3x) (all chemicals from Sigma-Aldrich). Subsequently, aminosilanized samples were immersed into a 7.5 mM solution of *N*-succinimidyl-3-maleimidopropionate in DMF for 1h under agitation at room temperature. The cross-linked samples were rinsed in DMF (3x), acetone (1x), distilled water (10x), ethanol (3x), acetone (3x) and dried with nitrogen.

Biofunctionalization

Biofunctionalization with linRGD, cRGD and CAS was carried out both on non-silanized (for physisorption) and silanized (for covalent functionalization) metal samples. 100µl of linRGD (100 µM in PBS), cRGD (100 µM in PBS), or CAS (100 µg/m in PBS) were added to the metal samples and incubated overnight at room temperature. After incubation, samples were

rinsed three times with PBS and blocked for 30 min with 1% BSA (Bovine Serum Albumin, Sigma Aldrich). Finally, samples were rinsed three times with PBS and sterilized with 70% ethanol for 30 min.

Surface characterization by Atomic Force Microscopy

Atomic force microscopy (AFM) imaging was carried out using a JPK NanoWizard III (JPK Instruments AG, Germany) operated in AC mode under dry conditions, using ACTA cantilevers (spring constant ~37 N/m, resonance frequency ~300 kHz; App Nano) at scan rates of 2 Hz. Nanolithography was performed in selected areas by scanning repeatedly (8-10 times) and rapidly (scan rate 20 lines/s) using high forces of typically > 20 nN to remove surface bound molecules. Images were analyzed and processed with Gwyddion (Gwyddion – Free SPM, sourceforge.net). Data representation was facilitated by OriginPro 8 (OriginLab Corporation, US) and CorelDraw X5 (Corel Corporation, CA).

Cell culture

Rat mesenchymal stem cells (rMSCs) were isolated from young Lewis rat femurs (2-4 weeks old) at the Institute for Bioengineering of Catalonia (IBEC) following the protocol described by González-Vázquez et al [47]. The expression profile of isolated cells was previously characterized to ensure mesenchymal stem cell phenotype [48]. Cells were cultured in Advanced DMEM (Sigma-Aldrich, Germany) supplemented with 10% (v/v) foetal bovine serum (FBS, Invitrogen), 20 mM HEPES Buffer solution (Invitrogen), antibiotics (50 U/mL penicillin, 50 µg/mL streptomycin, Invitrogen) and 2 mM L-glutamine (Invitrogen). Cultures were maintained in a humidified atmosphere with 5% CO_2 at 37° C. TrypLE™ Express (1x), phenol red (Invitrogen) was used for trypsinization. The medium used for the force adhesion assays was deprived from FBS and cells were used between passage 5 and 8.

Single-cell force spectroscopy assay

In order to quantify cell adhesion on different samples at the level of single cells, single-cell force spectroscopy was employed. Ti samples were tested first, as Ti is a well-known material, then adhesion on TiNbHf samples was tested. Cantilevers (MLCT, Bruker, Germany) were cleaned with acetone and calibrated in a fluid chamber (BioCell, JPK Instruments) in sterile PBS at room temperature following the thermal noise method implemented in the JPK AFM software. Cantilever functionalization was carried out according to a standard protocol [41]. In brief, cantilevers were incubated with BSA-biotin (0.5 mg/ml in PBS, Sigma, Germany) overnight at 37 ˚C in a parafilm-wrapped Petri dish. After extensive washing with PBS, the cantilevers were incubated in streptavidin (0.5 mg/ml in PBS; S4762, Sigma, Germany) at room temperature for 10 min. After another washing step in PBS, cantilevers were incubated with biotin-concanavalin A (0.2 mg/ml in PBS, Sigma, Germany) at room temperature for 10 min.

For cell adhesion force measurements, one Ti and one Ti alloy sample, both coated with the same peptide or protein, were glued into the same Petri dish using biocompatible epoxy (Reprorubber® Thin Pour, Flexbar, US). The free space of the Petri dish was incubated with PLL20[kDa]-g-PEG[3.5]-PEG2[kDa] (SurfaceSolutions, Switzerland) in HEPES (Sigma-Aldrich) at room temperature for 20 min to prevent cell attachment [49]. After rinsing several times with PBS, 2 ml serum-free culture medium was added. The experiment was carried out at about 36 ˚C using a heated fluid chamber (PetriDishHeater^{TM}, JPK Instruments, Germany). A NanoWizard III (JPK Instruments, Germany) was used for the force measurements. Prior to fishing for a cell, cantilever sensitivity was determined again. Right after pipetting a drop of cell suspension far away from the samples onto the PLL20[kDa]-g-PEG[3.5]-PEG2[kDa] coated area of the Petri dish, a cantilever was made to approach a floating, middle-sized cell and held in contact for a few seconds [50]. After a cell was successfully attached to the cantilever, the cantilever was lifted upwards and the cell was allowed to relax for a couple of minutes before cell adhesion force experiments were started. Cells were then brought into contact with the sample up to a contact force of 0.5 nN and the cantilever position was held constant for 5 sec (constant height mode). The extension and retraction speeds were 3 µm/s.

Force-extension curves were measured on both samples with one and the same cell. About 20 curves were obtained at different locations on each sample, with > 6 cells for each sample type. Force-extension curves were analyzed with the JPK SPM data processing software (JPK Instruments, Germany). The average cell detachment force, i.e. the force needed to initiate cell detachment, and the detachment energy were calculated for each cell and the results were plotted using boxplots in Origin 9.0 (Originlab, USA).

Colorimetric and fluorescence-based cell adhesion assays

10000 cells per well were seeded onto the biofunctionalized Ti and TiNbHf discs and allowed to adhere for 4 h at 37 ºC in a 5 % CO_2 atmosphere at 95% relative humidity. Afterwards, the cell culture medium was removed and each well was rinsed three times with PBS.

After incubation, 300 µl of mammalian protein extraction reagent (M-PER Thermo Fisher, Illinois, USA) were added to the samples. The Cytotoxicity Detection Kit ^{PLUS} (LDH) (Roche, USA) was used to determine the number of adhered cells on the samples following the manufacturer's instructions. The LDH test is a non-radioactive colorimetric assay based on the measurement of the lactate dehydrogenase activity released from the cytosol of lysed cells. LDH activity is proportional to the number of lysed cells according to a calibration curve prepared with a decreasing number of cells.

For cell morphology inspection samples were fixed with 4% paraformaldehyde (Sigma-Aldrich) for 30 min and washed three times with PBS. Fixed cells were permeabilized with Triton X-100 (Sigma-Aldrich) at 0.05% in PBS for 20 min and cleaned with 20 mM glycine (Sigma-Aldrich) in a PBS solution three times. To reduce non-specific binding, samples were blocked with 1% BSA (Sigma-Aldrich) in PBS and incubated for 30 min. TRITC-phalloidin (Invitrogen, Spain) at a dilution 1:300 in PBS was added to each sample and incubated in the dark for 1 h. After incubation, samples were rinsed three times with 20 mM glycine in PBS. 300 µl DAPI (1:1000 in PBS, Invitrogen, Spain) were added to each sample and incubated in the dark for 2 min. Samples were rinsed three times with 20 mM glycine in PBS. Samples were placed on a cover slide with 8 µl of Mowiol® 4-88 (Sigma-Aldrich) as anti-fading agent

and visualized in an E600 fluorescence microscope (Nikon Corp., Japan). Cells cultured onto coverslips were used as control.

Results and discussion

Physisorption of cRGD and CAS on Ti and TiNbHf surfaces

Figure 1 shows AFM topography images of cRGD and CAS physisorbed onto Ti and the TiNbHf alloy (Figs. 1B, C, E, F), as well as control images taken on uncoated Ti (Fig. 1A) and TiNbHf (Fig. 1D). linRGD, which contains the same cell-binding sequence and spacer-anchor units as cRGD, was not considered in this study. Physisorption of individual cRGD molecules on both materials is visible but does not yield dense surface coverage (Figs. 1 B, E). Indeed, only isolated spots are observed with averaged heights of 1-3 nm. In contrast, physisorption of the higher molecular weight CAS leads to a closed monolayer formation with a thickness of about 10 nm (Figs. 1C, F), as revealed by *in situ* AFM nanolithography, which was used to scratch a quadratic mark into the protein layer. We determined the same thickness of about 10 nm for a monolayer of CAS molecules adsorbed to freshly cleaved mica (Suppl. Fig. 1). As expected, this layer thickness is much smaller than the size of full fibronectin [51, 52].

Covalent binding of cRGD and CAS to Ti and TiNbHf surfaces

Recombinant fragments of proteins are conventionally bound to surfaces by physisorption [53], brushed polymers [25] or self-assembled monolayers of alkanethiols [54, 55]. Here we applied a different approach, which is based on silanization of the surfaces with APTES followed by crosslinking with *N*-succinimidyl-3-maleimidopropionate. Maleimide groups present at the surface can readily react with nucleophilic thiol and amino groups present on RGD and CAS molecules, respectively, establishing stable covalent bonds. Hence, silanization should be a tethering method of surface functionalization with higher efficiency and stability than physisorption. Figure 2 presents AFM images of cRGD and CAS covalently bound to Ti and TiNbHf surfaces following this approach. Surfaces appear to be coated both with cRGD and CAS, as demonstrated by nanolithography. In contrast to the AFM experiments on physisorbed

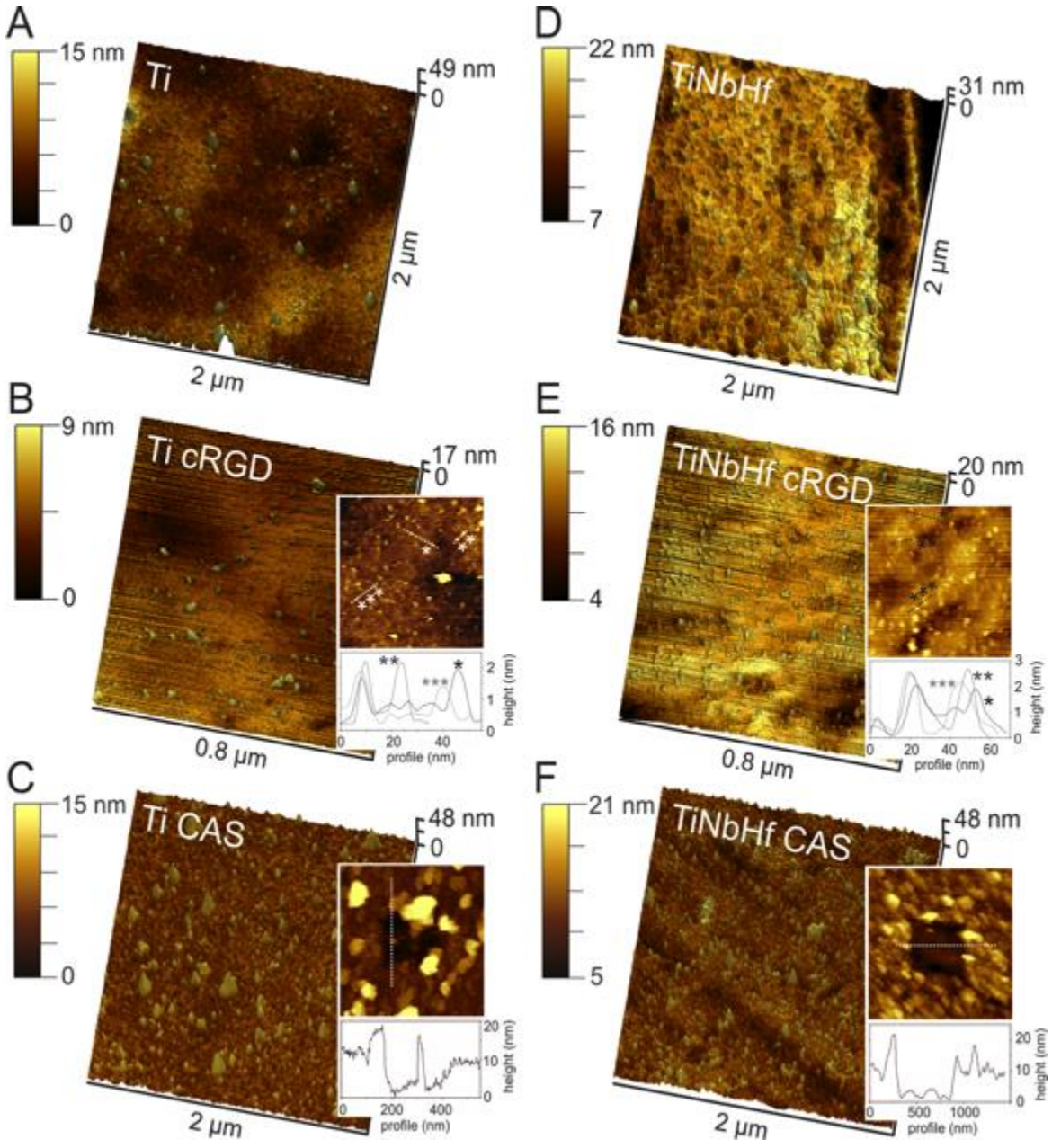

Fig. 1 AC mode AFM images of uncoated control samples made from Ti (A) and TiNbHf (D) as well as for cRGD and CAS physisorbed to Ti (B, C) and TiNbHf (E, F), respectively. The controls (A, D) show that there is significant intrinsic roughness for both materials, particularly for the TiNbHf alloy. Insets show areas where nanolithography was carried out. Height profiles show surface topography along the lines marked in the insets. Whereas physisorption of cRGD does not lead to a closed peptide layer, CAS forms a dense monolayer on both surfaces as proven by *in situ* AFM nanolithography, revealing a coating depth for CAS of about 10 nm consistently on Ti and TiNbHf.

cRGD, here a significant and homogeneous coverage of the surfaces with cRGD was observed. The layer of CAS chemisorbed on the surfaces is also rather homogeneous with a thickness value of about 10 nm, slightly higher than that observed for the cRGD layer.

The height profiles shown in Fig. 2 A and C indicate that the cRGD layer is a few nm thicker on TiNbHf than on Ti, but as the intrinsic roughness of both materials cannot be neglected, it is hard to determine the true layer thickness. Still, as the cRGD layer is significantly thicker than 1 nm, it can be assumed that a multilayer of cRGD is bound to the surface.

CAS was present on both the Ti and the TiNbHf in seemingly homogeneous layers, which to some extent even equalized the intrinsic roughness of these materials. CAS molecules did not show a defined conformation on the surfaces, in contrast to the fibril-like distribution observed by Rico et al. on poly(ethyl acrylate) surfaces [55]. Such effects might be explained by changes in the topographical features and physicochemical properties of the surfaces. As a matter of fact, studies by Zhang et al. showed that both protein adsorption and conformational changes are strongly influenced by these surface properties [56].

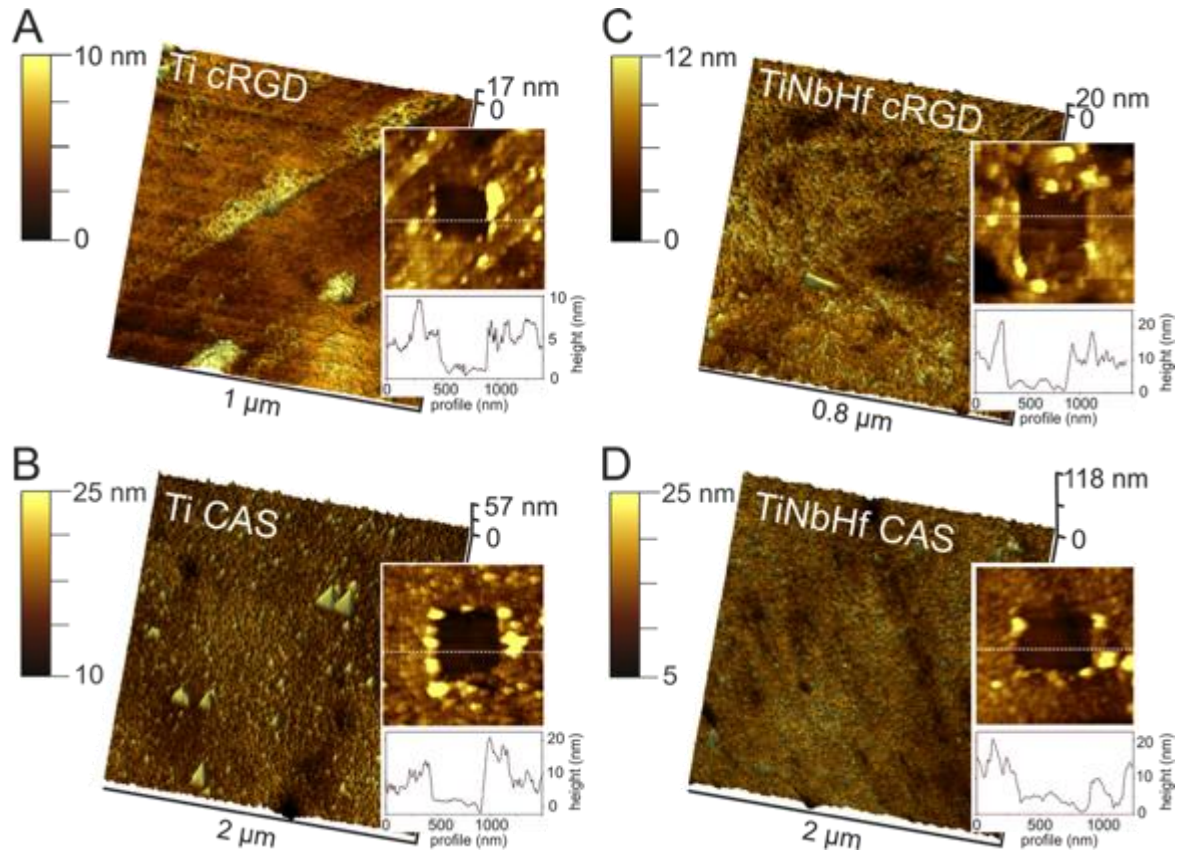

Fig. 2 AC mode AFM images after covalent binding of cRGD onto Ti (A) and TiNbHf (C) surfaces, and of CAS onto Ti (B) and TiNbHf (D), respectively. Nanolithography (insets) reveals the success of the functionalization process both for cRGD and CAS.

Cell detachment forces are controlled by surface biofunctionalization

Single-cell force spectroscopy has the great potential to quantify cell-surface interactions in detail at the level of single cells and even at the sub-cellular level down to the single molecule regime. Figure 3 shows representative force-extension curves of a rMSC retracted from surfaces coated with cRGD and CAS after 5 sec of cell-surface interaction. This experiment proved the existence of specific molecular interactions between the cell and the surface, as many individual rupture events (distinct steps) are present in the force curves. In particular the CAS coating leads to many rupture events and high cell detachment forces of more than 1 nN.

Cell detachment forces were determined for surfaces on which linRGD, cRGD and CAS were covalently coupled to the surfaces of Ti and TiNbHf. Silanization was chosen as the immobilization method because it yielded more homogenous coatings than physisorption.

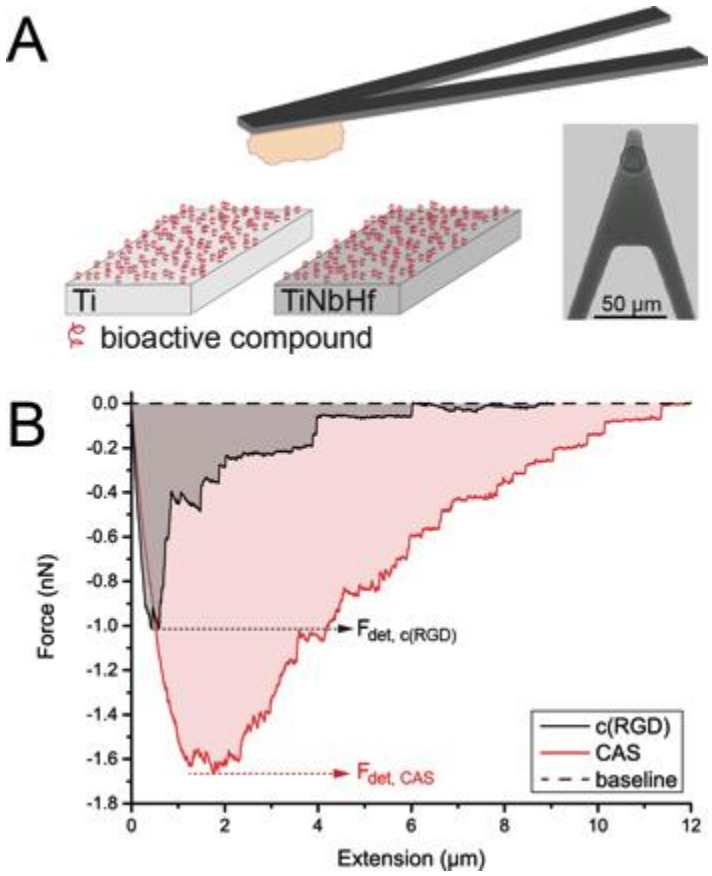

Fig. 3 (A) Sketch of the experimental situation. A cell is attached to the cantilever (inset) and cell adhesion is characterized on biofunctionalized Ti and TiNbHf. (B) Force-extension curves for the detachment of a rMSC from a TiNbHf alloy coated with cRGD (black) and CAS (red). The dashed black line indicates the baseline. Individual molecular ruptures are evident from distinct force steps in the curve. The shaded area under each curve represents the work of detachment. The force needed to initiate cell detachment is called detachment force (F_{det}, arrows) and is significantly smaller for c(RGD) in comparison to CAS.

Moreover, covalent coupling was essential in order to avoid the loss of the coating molecules from the surface during cell detachment experiments. Fig. 4 summarizes cell detachment forces obtained for Ti and TiNbHf functionalized with linRGD, cRGD or CAS in boxplots. The data clearly show that the coating of both Ti and TiNbHf with CAS leads to highest cell adhesion forces, followed by cRGD functionalization. Smallest adhesion forces were measured for surfaces coated with linRGD, which is in agreement with the lower binding affinity described for linRGD [35].

A similar influence of the surface coating was obtained for the work of cell detachment (Fig. 4B). In particular, our data indicate slightly higher cell detachment forces for the biofunctionalized TiNbHf alloy compared to Ti surface; however, as the obtained force distributions are rather broad, this difference is not very significant. Furthermore, the broad

force distributions might not only be caused by biological differences between different cells, but also by the non-homogeneous surface roughness of the raw materials and the partly non-homogeneous surface coating. In particular for the coating of TiNbHf with cRGD and of Ti with CAS, strong molecular clustering and thus a rather inhomogeneous surface coating is visible in the AFM topography images (Fig. 3), which is also reflected in the broad cell detachment force distributions (Fig. 4A).

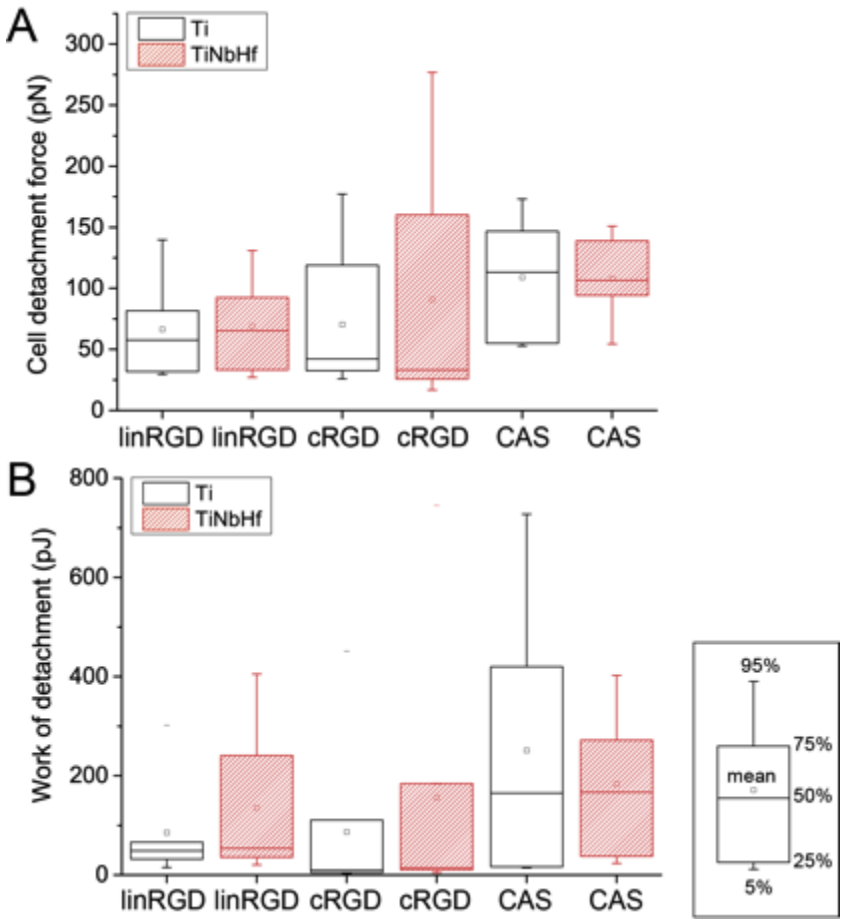

Fig. 4 Cell detachment force (A) and work of detachment (B) measured on Ti and TiNbHf substrates covalently biofunctionalized with linRGD (100 µM), cRGD (100 µM), and CAS (100 µg/ml). Box plots (n=6, 20 replicates) are used to show the distribution of forces measured from individual cells. The bottom and top of the box are the first and third quartiles (25%-75%) of measured forces, whiskers (-) represent 5-95% data spreading. The line inside the box is the median value of each distribution, the little square (☐) represents the mean. Clearly, cell adhesion forces at 5 sec cell-surface contact time are highest when the surfaces are coated with CAS and for cRGD. A similar trend can be observed for the work of detachment. Histograms showing the full distribution of forces are given in the Supplementary Information.

The highest values of cell detachment forces were observed for CAS covalently bound to Ti and to the TiNbHf alloy. This is easy to explain, as the CAS fragment spans the region from 8th to 10th type III of fibronectin including the sequences RGD (Arg-Gly-Asp) and PHSRN (Pro-

His-Ser-Arg-Asn). The PHSRN sequence is needed to achieve full adhesive activity for the $\alpha_5\beta_1$ integrin receptor. Previous research has shown that high affinity binding requires this synergy site to be engaged [57, 58], and that availability of both the synergy site and RGD has significant impact on cell adhesion [38, 59]. Hence, CAS is clearly superior to RGD in initial cell adhesion.

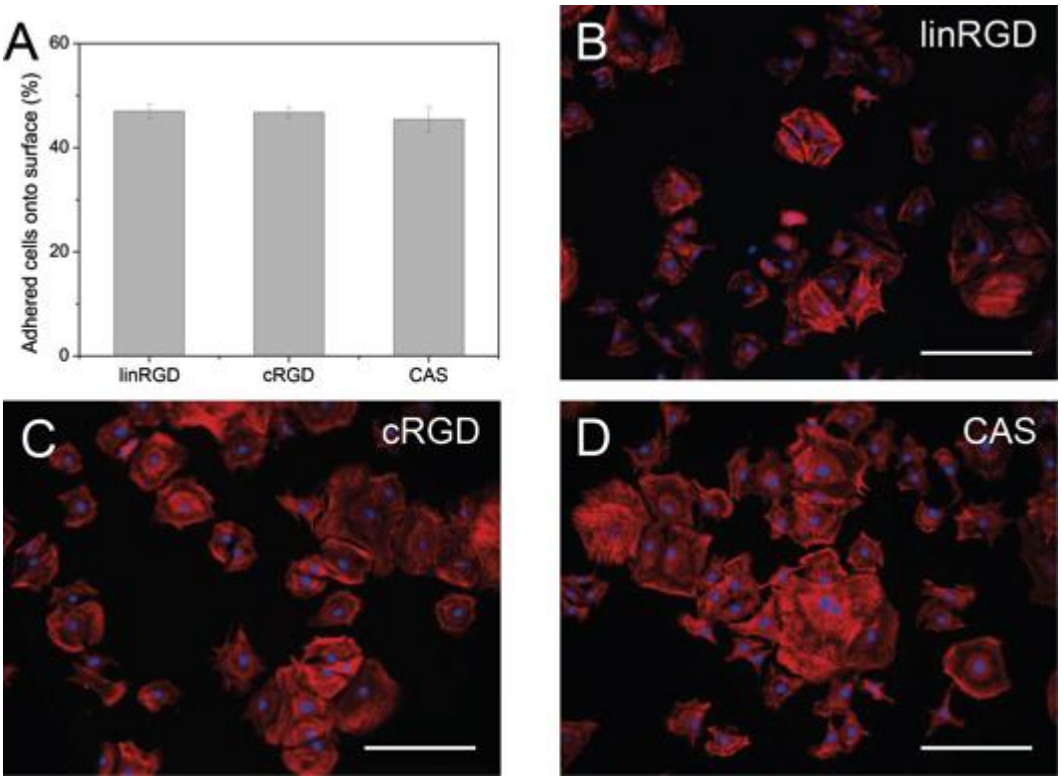

Fig. 5 A) Percentage (error bars: SD, n=5) of cells adhered on the TiNbHf alloy covalently functionalized with linRGD 100 µM , cRGD 100 µM and CAS 100 µg/ml. This result shows that the number of adhering cells is not influenced by the type of bioactive coating provided on the TiNbHf surface. (B)-(D) Immunofluorescence images of cells on TiNbHf surfaces covalently biofunctionalized with linRGD 100 µM (B), cRGD 100 µM (C) and CAS 100 µg/ml (D). Actin filaments are shown in red and the nucleus in blue. Scalebars: 200 µm.

Influence of biofunctionalization on cell number and morphology

The number of rMSCs adhering to our TiNbHf alloy after 4 h incubation time was determined by an LDH assay. In particular, we compared the effect of our three different biofunctionalization types, i.e. covalent coating with linRGD, cRGD and CAS. Figure 5A shows the percentage of adherent cells on samples functionalized with linRGD, cRGD and

CAS. Interestingly, there is no difference in the number of adherent cells between the different surface coatings.

Representative images of MSCs after 4h of adhesion on TiNbHf substrates covalently coated with different bioactive molecules are shown in Fig. 5. In general, cells cultured on functionalized surfaces are more spread compared to cells cultured on coverslips (Supplementary Figure 3), where cells exhibit the typical spindle-shape morphology. This change in cell morphology could be attributed to higher availability of cell adhesive moieties per area. Whereas cells adhering to linRGD functionalized substrates have only little organization of actin into actin stress fibers (Fig. 5B), more actin stress fibers are present on surfaces coated with cRGD (Fig. 5C) and the higher organization of actin stress fibers and cell spreading is observed for CAS coating (Fig. 5D). This is consistent with the results obtained for cell detachment forces.

Conclusions

The importance of Ti and its alloys for biomedical implants is immense and coating with bioactive compounds can improve the biointegration capacity of these medically highly important metals. We investigated the topography of Ti and Ti25Nb21Hf alloys coated with linRGD, cRGD and fibronectin fragment (CAS). Two coating strategies, physisorption and covalent binding through silanization, were investigated and AFM topography and nanolithography experiments clearly showed that covalent coating methods are a suitable strategy for achieving homogeneous surface coatings. Single-cell force spectroscopy experiments confirmed quantitatively the significant adhesion promoting effect of CAS on cell adhesion even at the single cell level, reflecting the high potential of single-cell force spectroscopy for quantifiying cell adhesion on biomaterials. Clearly, the fibronectin fragment (CAS) led to the strongest cell adhesion compared to linRGD and cRGD and immunofluorescence experiments confirmed that this also causes prominent actin stress fiber formation, indicating firm cell adhesion and thus, higher osseoingration potential. Hence, we can conclude that covalent biofunctionalization of Ti and Ti25Nb21Hf with CAS (fibronectin

fragment $FNIII_{8-10}$) is a functional method for improving the biointegration potential of Ti-based implant materials. Moreover, suitable surface functionalization can have high impact for Ti25Nb21Hf, which is an increasingly important novel biomaterial in the field.

Acknowledgements

We thank Sören Gutekunst and Laith Kadem for their support with silanization chemistry and with the plasma machine, and Manuela Lieb for support with cell culture. Furthermore, Q. L. and C. S.-U. acknowledge the Deutsche Forschungsgemeinschaft (DFG; SFB 677 (project B11) and grant SE 1801/2-1). C. L. acknowledges funding by the Marie Skłodowska Curie Actions Intra European Fellowship PIEF-GA-2012-330418. C.H.D would like to thank the Spanish Government for financial support through MAT2012-30706 project co-funded by the EU through European Regional Development Funds, the FI fellowship of the AGAUR agency and the CIBER-BBN mobility funding. C. M.-M. thanks the support of the Government of Catalonia (2011-BP-B-00042) and the People Programme (Marie Curie Actions) of the European Union's FP7 (PEOPLE-2012-CIG, REA Grant Agreement 321985). Bill Brook Shurtleff is acknowledged for proofreading the manuscript.

References

[1] M. Niinomi, Mechanical properties of biomedical titanium alloys, Materials Science and Engineering: A, 243 (1998) 231-236.

[2] S.H. Swierenga, J.P. Gilman, J.R. McLean, Cancer risk from inorganics, Cancer Metast Rev, 6 (1987) 113-154.

[3] M. Uo, F. Watari, A. Yokoyama, H. Matsuno, T. Kawasaki, Dissolution of nickel and tissue response observed by X-ray scanning analytical microscopy, Biomaterials, 20 (1999) 747-755.

[4] S. Yumoto, H. Ohashi, H. Nagai, S. Kakimi, Y. Ogawa, Y. Iwata, K. Ishii, Aluminum neurotoxicity in the rat brain, International Journal of PIXE, 02 (1992) 493-504.

[5] M. Niinomi, Recent metallic materials for biomedical applications, Metall and Mat Trans A, 33 (2002) 477-486.

[6] Y. Ke, R. Yibin, Nickel-free austenitic stainless steels for medical applications, Science and Technology of Advanced Materials, 11 (2010) 014105.

[7] H. Matsuno, A. Yokoyama, F. Watari, M. Uo, T. Kawasaki, Biocompatibility and osteogenesis of refractory metal implants, titanium, hafnium, niobium, tantalum and rhenium, Biomaterials, 22 (2001) 1253-1262.

[8] K.Y. Xie, Y. Wang, Y. Zhao, L. Chang, G. Wang, Z. Chen, Y. Cao, X. Liao, E.J. Lavernia, R.Z. Valiev, B. Sarrafpour, H. Zoellner, S.P. Ringer, Nanocrystalline β-Ti alloy with high hardness, low Young's modulus and excellent in vitro biocompatibility for biomedical applications, Materials Science and Engineering: C, 33 (2013) 3530-3536.

[9] M. González, J. Peña, J.M. Manero, M. Arciniegas, F.J. Gil, Design and Characterization of New Ti-Nb-Hf Alloys, J. of Materi Eng and Perform, 18 (2009) 490-495.

[10] M. Morinaga, M. Yukawa, H. Adachi, H. Ezaki, Superalloys, AIME1984.

[11] M. Morinaga, e. al., Conference San Diego.

[12] M. Arciniegas, J. Pena, J.M. Manero, J.C. Paniagua, F.J. Gil, Quantum parameters for guiding the design of Ti alloys with shape memory and/or low elastic modulus, Philosophical Magazine, 88 (2008) 2529-2548.

[13] C. Herranz-Diez, F. Gil, J. Guillem-Marti, J. Manero, Mechanical and physicochemical characterization along with biological interactions of a new Ti25Nb21Hf alloy for bone tissue engineering., J. Biomater. Appl., (2015) 0885328215577524.

[14] J. Guillem-Martí, C. Herranz-Díez, J.E. Shaffer, F.J. Gil, J.M. Manero, Mechanical and microstructural characterization of new nickel-free low modulus β-type titanium wires during thermomechanical treatments, Materials Science and Engineering: A, 636 (2015) 507-515.

[15] M. González, E. Salvagni, J.C. Rodríguez-Cabello, E. Rupérez, F.J. Gil, J. Peña, J.M. Manero, A low elastic modulus Ti-Nb-Hf alloy bioactivated with an elastin-like protein-based polymer enhances osteoblast cell adhesion and spreading, Journal of Biomedical Materials Research Part A, 101A (2013) 819-826.

[16] S. Bauer, P. Schmuki, K. von der Mark, J. Park, Engineering biocompatible implant surfaces: Part I: Materials and surfaces, Progress in Materials Science, 58 (2013) 261-326.

[17] F.R. Maia, S.J. Bidarra, P.L. Granja, C.C. Barrias, Functionalization of biomaterials with small osteoinductive moieties, Acta Biomaterialia, 9 (2013) 8773-8789.

[18] B. Zhang, D. Myers, G. Wallace, M. Brandt, P. Choong, Bioactive Coatings for Orthopaedic Implants—Recent Trends in Development of Implant Coatings, International Journal of Molecular Sciences, 15 (2014) 11878-11921.

[19] M. Geetha, A.K. Singh, R. Asokamani, A.K. Gogia, Ti based biomaterials, the ultimate choice for orthopaedic implants – A review, Progress in Materials Science, 54 (2009) 397-425.

[20] A.J. García, C.D. Reyes, Bio-adhesive Surfaces to Promote Osteoblast Differentiation and Bone Formation, Journal of Dental Research, 84 (2005) 407-413.

[21] T.-I. Kim, J.-H. Jang, C.-P. Chung, Y. Ku, Fibronectin fragment promotes osteoblast-associated gene expression and biological activity of human osteoblast-like cell, Biotechnology Letters, 25 (2003) 2007-2011.

[22] F.J. Arias, V. Reboto, S. Martín, I. López, J.C. Rodríguez-Cabello, Tailored recombinant elastin-like polymers for advanced biomedical and nano(bio)technological applications, Biotechnology Letters, 28 (2006) 687-695.

[23] V. Paredes, E. Salvagni, E. Rodríguez-Castellon, F.J. Gil, J.M. Manero, Study on the use of 3-aminopropyltriethoxysilane and 3-chloropropyltriethoxysilane to surface biochemical modification of a novel low elastic modulus Ti–Nb–Hf alloy, Journal of Biomedical Materials Research Part B: Applied Biomaterials, (2014) n/a-n/a.

[24] R. Fraioli, F. Rechenmacher, S. Neubauer, J.M. Manero, J. Gil, H. Kessler, C. Mas-Moruno, Mimicking bone extracellular matrix: Integrin-binding peptidomimetics enhance osteoblast-like cells adhesion, proliferation, and differentiation on titanium, Colloids and Surfaces B: Biointerfaces, 128 (2015) 191-200.

[25] T.A. Petrie, J.E. Raynor, C.D. Reyes, K.L. Burns, D.M. Collard, A.J. García, The effect of integrin-specific bioactive coatings on tissue healing and implant osseointegration, Biomaterials, 29 (2008) 2849-2857.

[26] Y. Zhang, Q. Xiang, S. Dong, C. Li, Y. Zhou, Fabrication and characterization of a recombinant fibronectin/cadherin bio-inspired ceramic surface and its influence on adhesion and ossification in vitro, Acta Biomaterialia, 6 (2010) 776-785.

[27] S. Goennenwein, M. Tanaka, B. Hu, L. Moroder, E. Sackmann, Functional Incorporation of Integrins into Solid Supported Membranes on Ultrathin Films of Cellulose: Impact on Adhesion, Biophysical Journal, 85 (2003) 646-655.

[28] U. Hersel, C. Dahmen, H. Kessler, RGD modified polymers: biomaterials for stimulated cell adhesion and beyond, Biomaterials, 24 (2003) 4385-4415.

[29] J.L. Sechler, H. Rao, A.M. Cumiskey, I. Vega-Colón, M.S. Smith, T. Murata, J.E. Schwarzbauer, A novel fibronectin binding site required for fibronectin fibril growth during matrix assembly, The Journal of Cell Biology, 154 (2001) 1081-1088.

[30] M. Zink, F. Szillat, U. Allenstein, S.G. Mayr, Interaction of Ferromagnetic Shape Memory Alloys and RGD Peptides for Mechanical Coupling to Cells: from Ab Initio Calculations to Cell Studies, Advanced Functional Materials, 23 (2013) 1383-1391.

[31] M. Arnold, E.A. Cavalcanti-Adam, R. Glass, J. Blümmel, W. Eck, M. Kantlehner, H. Kessler, J.P. Spatz, Activation of Integrin Function by Nanopatterned Adhesive Interfaces, ChemPhysChem, 5 (2004) 383--388.

[32] H.C. Kroese-Deutman, J. van den Dolder, P.H. Spauwen, J.A. Jansen, Influence of RGD-loaded titanium implants on bone formation in vivo., Tissue Eng. , 11 (2005) 1867-1875.

[33] F. Rechenmacher, K. Steigerwald, B. Laufer, S. Neubauer, T.G. Kapp, L. Li, C. Mas-Moruno, M. Joner, H. Kessler, The Integrin Ligand c(RGDf(NMe)Nal) Reduces Neointimal

Hyperplasia in a Polymer-Free Drug-Eluting Stent System, ChemMedChem, 9 (2014) 1413-1418.

[34] M. Kantlehner, P. Schaffner, D. Finsinger, J. Meyer, A. Jonczyk, B. Diefenbach, B. Nies, G. Hölzemann, S.L. Goodman, H. Kessler, Surface Coating with Cyclic RGD Peptides Stimulates Osteoblast Adhesion and Proliferation as well as Bone Formation, ChemBioChem, 1 (2000) 107-114.

[35] R. Haubner, D. Finsinger, H. Kessler, Stereoisomeric Peptide Libraries and Peptidomimetics for Designing Selective Inhibitors of the α v β 3 Integrin for a New Cancer Therapy, Angew. Chem. Int. Ed., 36 (1997) 1374-1389.

[36] D.A. Puleo, R. Bizios, Biological Interactions on Materials Surfaces, Springer-Verlag New York, 2009.

[37] M. Kantlehner, D. Finsinger, J. Meyer, P. Schaffner, A. Jonczyk, B. Diefenbach, B. Nies, H. Kessler, Selective RGD-Mediated Adhesion of Osteoblasts at Surfaces of Implants, Angewandte Chemie International Edition, 38 (1999) 560-562.

[38] F.C. Schenk, H. Boehm, J.P. Spatz, S.V. Wegner, Dual-Functionalized Nanostructured Biointerfaces by Click Chemistry, Langmuir, 30 (2014) 6897-6905.

[39] S.M. Cutler, Garcı, amp, x, A.J. a, Engineering cell adhesive surfaces that direct integrin α 5 β 1 binding using a recombinant fragment of fibronectin, Biomaterials, 24 (2003) 1759-1770.

[40] N. Walter, C. Selhuber, J. Blümmel, H. Kessler, J.P. Spatz, Cellular Unbinding Forces of Initial Adhesion Processes on Nanopatterned Surfaces Probed with Magnetic Tweezers, Nano Lett., 6 (2006) 398-402.

[41] C. Selhuber-Unkel, M. López-García, H. Kessler, J.P. Spatz, Cooperativity in Adhesion Cluster Formation during Initial Cell Adhesion, Biophys. J., 95 (2008) 5424-5431.

[42] A.V. Taubenberger, D.W. Hutmacher, D.J. Muller, Single-Cell Force Spectroscopy, an Emerging Tool to Quantify Cell Adhesion to Biomaterials, Tissue Engineering Part B: Reviews, 20 (2013) 40-55.

[43] F. Albericio, Developments in peptide and amide synthesis, Current Opinion in Chemical Biology, 8 (2004) 211-221.

[44] C. Mas-Moruno, R. Fraioli, F. Albericio, J.M. Manero, F.J. Gil, Novel Peptide-Based Platform for the Dual Presentation of Biologically Active Peptide Motifs on Biomaterials, ACS Applied Materials & Interfaces, 6 (2014) 6525-6536.

[45] M. Pfaff, Tangemann, K., B. Müller, M. Gurrath, G. Müller, H. Kessler, R. Timpl, J. Engel, Selective Recognition of Cyclic RGD Peptides of NMR Defined Conformation by alphaIIbbeta3, alphaVbeta3, and alpha5beta1 Integrins, J. Biol. Chem., 269 (1994) 20233-20238.

[46] C. Mas-Moruno, P.M. Dorfner, F. Manzenrieder, S. Neubauer, U. Reuning, R. Burgkart, H. Kessler, Behavior of primary human osteoblasts on trimmed and sandblasted Ti6Al4V

surfaces functionalized with integrin α v β 3-selective cyclic RGD peptides, Journal of Biomedical Materials Research Part A, 101A (2013) 87-97.

[47] A. González-Vázquez, J.A. Planell, E. Engel, Extracellular calcium and CaSR drive osteoinduction in mesenchymal stromal cells, Acta Biomaterialia, 10 (2014) 2824-2833.

[48] A. Aguirre, J.A. Planell, E. Engel, Dynamics of bone marrow-derived endothelial progenitor cell/mesenchymal stem cell interaction in co-culture and its implications in angiogenesis, Biochemical and Biophysical Research Communications, 400 (2010) 284-291.

[49] J.W. Lussi, D. Falconnet, J.A. Hubbell, M. Textor, G. Csucsd, Pattern stability under cell culture conditions - A comparative study of patterning methods based on PLL-g-PEG background passivation, Biomaterials, 27 (2006) 2534-2541.

[50] M. Benoit, C. Selhuber-Unkel, Measuring cell adhesion forces: theory and principles, Methods in molecular biology (Clifton, N.J.), 736 (2011) 355-377.

[51] M. Bergkvist, J. Carlsson, S. Oscarsson, Surface-dependent conformations of human plasma fibronectin adsorbed to silica, mica, and hydrophobic surfaces, studied with use of Atomic Force Microscopy, Journal of Biomedical Materials Research Part A, 64A (2003) 349-356.

[52] J.R. Hull, G.S. Tamura, D.G. Castner, Structure and Reactivity of Adsorbed Fibronectin Films on Mica, Biophysical Journal, 93 (2007) 2852-2860.

[53] M. Salmerón-Sánchez, P. Rico, D. Moratal, T.T. Lee, J.E. Schwarzbauer, A.J. García, Role of material-driven fibronectin fibrillogenesis in cell differentiation, Biomaterials, 32 (2011) 2099-2105.

[54] T.A. Petrie, J.R. Capadona, C.D. Reyes, A.J. García, Integrin specificity and enhanced cellular activities associated with surfaces presenting a recombinant fibronectin fragment compared to RGD supports, Biomaterials, 27 (2006) 5459-5470.

[55] P. Rico, C. González-García, T.A. Petrie, A.J. García, M. Salmerón-Sánchez, Molecular assembly and biological activity of a recombinant fragment of fibronectin (FNIII7–10) on poly(ethyl acrylate), Colloids and Surfaces B: Biointerfaces, 78 (2010) 310-316.

[56] H. Zhang, K. Bremmell, S. Kumar, R.S.C. Smart, Vitronectin adsorption on surfaces visualized by tapping mode atomic force microscopy, Journal of Biomedical Materials Research Part A, 68A (2004) 479-488.

[57] S. Aota, M. Nomizu, K.M. Yamada, The short amino acid sequence Pro-His-Ser-Arg-Asn in human fibronectin enhances cell-adhesive function, Journal of Biological Chemistry, 269 (1994) 24756-24761.

[58] A.K. Dillow, S.E. Ochsenhirt, J.B. McCarthy, G.B. Fields, M. Tirrell, Adhesion of α 5 β 1 receptors to biomimetic substrates constructed from peptide amphiphiles, Biomaterials, 22 (2001) 1493-1505.

[59] F. Li, S.D. Redick, H.P. Erickson, V.T. Moy, Force Measurements of the α (5) β (1) Integrin–Fibronectin Interaction, Biophysical Journal, 84 (2003) 1252-1262.